Rigorous design of an ultra-high Q/V photonic/plasmonic cavity to be used in biosensing applications

Rigorous design of an ultra-high Q/V photonic/plasmonic cavity to be used in biosensing applications

Highlights

- A device based on a PhC dielectric cavity vertically coupled to a plasmonic slot is proposed.
- The rigorous design of the device was carried out by using the 3D Finite Element Method.
- A Q/V ratio = $10^7 (\lambda/n)^{-3}$ was achieved due to the high confinement in the cavity.
- The strong light-matter interaction makes the hybrid cavity suitable for biosensing.

Rigorous design of an ultra-high Q/V photonic/plasmonic cavity to be used in biosensing applications

D. Conteduca, F. Dell'Olio, F. Innone, C. Ciminelli, M. N. Armenise

The Authors are with the Optoelectronics Laboratory, Politecnico di Bari, Via Re David 200, 70125 Bari, Italy,

(corresponding author: phone: +39 080 5963270; fax: +39 080 5963610; e-mail: caterina.ciminelli@poliba.it)

***Abstract*—A hybrid device based on a 1D PhC dielectric cavity vertically coupled to a plasmonic slot is proposed for use in biosensing applications. Under efficient coupling conditions between the Bloch mode in the 1D PhC dielectric cavity and the surface plasmon polaritons mode in the metal slot, an ultra-high Q/V ratio (~ 10^7 $(\lambda/n)^{-3}$) has been achieved with a remarkable resonance transmission T (= 47%), due to high spectral and spatial confinement in the cavity. The rigorous design process of the cavity, including the influence of geometrical and physical parameters on its performance, has been carried out using the 3D Finite Element Method. A strong light-matter interaction was observed, making the photonic-plasmonic cavity suitable for biosensing and, in particular, for optical trapping of living matter at nanoscale, such as proteins and DNA sections, as required in several biomedical applications.**

Index Terms—Ultra-high Q/V, photonic crystal cavity, plasmonic slot, photonic/plasmonic cavity

1. INTRODUCTION

In recent years, optical resonant cavities have attracted remarkable attention due to the high values of Q-factor (Q) and the small mode volume (V) achievable. High values of the Q/V ratio correspond to strong light-matter interaction, making such devices suitable for several applications, such as biosensing, where high sensitivity is requested to detect very low sample concentrations [1-3]. In this field, optical trapping is an emerging application, allowing high value of optical forces to trap, detect and manipulate small particles, such as living cells, single particles and metal beads. Optical resonant

cavities can also be used in optical communication systems (e.g. optical filters and lasers) due to their low cost, low operating energy, and efficient control of emission rates [4-6].

Among the resonant cavities proposed in the literature, photonic crystal cavities (PhC) have demonstrated the highest performance in terms of Q/V ratio and small footprints.

While the highest experimental Q-factor (= $9x10^6$) [7] and a Q/V ratio of $3.2x10^6$ $(\lambda/n)^{-3}$ [8] have been obtained in 2D PhC cavities, in 1D PhC cavities, consisting of a single row of holes in a photonic wire, very high Q values up to 10^9 [9] and mode volume as low as 0.38 $(\lambda/n)^3$ have been demonstrated [10]. The 1D slotted PhC cavities, consisting of a photonic crystal wire with a central slot waveguide along the holes, have shown the strongest energy confinement, which corresponds to a very low mode volume (= $9x10^{-3}(\lambda/n)^3$) and Q/V ratio up to 10^7 $(\lambda/n)^{-3}$ [11]. However, such cavities are affected by a very low resonance transmission (T < 10%) due to the strong dielectric discontinuity in the slot that, at the same time, causes an enhancement of the field and an increase in the optical losses. The resonance transmission represents an important figure of merit for resonant cavities related to a good detection resolution. The best theoretical value of the Q/V ratio (~ 10^7 $(\lambda/n)^{-3}$) with a resonance transmission close to T = 30%, has been obtained in a 1D PhC dielectric cavity, even if the experimental results showed a lower Q-factor (~ $8x10^4$) and a Q/V ratio lower by about two orders of magnitude ($Q/V \sim 10^5(\lambda/n)^{-3}$) [12].

Strong light confinement and reductions in the mode volume are limited by the diffraction limit. Plasmonic cavities, in which the resonance mode of the surface plasmon polaritons (SPPs) is excited at the dielectric-metal interface, have been proposed to overcome this limit through a significant reduction of the mode volume, $V = 10^{-4}$ $(\lambda/n)^3$ [13-15], which is about two orders of magnitude smaller than the minimum value obtained by dielectric PhC cavities with a consequent improvement in light-matter interaction. This strong enhancement of the optical energy confinement in volumes at nanoscale has furthered the use of plasmonic cavities for several emerging applications, such as surface-enhanced spectroscopy, quantum cryptography, increasing the emission rate in silicon, optical trapping and biosensing [16-18]. Optical losses are the most critical issue for plasmonic cavities, only allowing very-low Q-factor values ($Q \sim 10^2$), which correspond to a $Q/V \sim 10^5$ $(\lambda/n)^{-3}$ [13].

A trade-off between the high spectral energy density of the PhC dielectric cavities and the strong spatial energy confinement of the plasmonic ones can be realized by hybrid cavities, i.e. photonic/plasmonic devices. Several configurations of photonic-plasmonic cavities have been proposed [19-22], and the highest Q/V ratio obtained is $8x10^{4}$ $(\lambda/n)^{-3}$ [21]. This value is much lower than that in dielectric cavities, but the most important advantage is related to the strong confinement of the optical energy in the medium with a lower refractive index [23]. Such performance makes hybrid cavities suitable for biosensing applications and optical trapping [24-26], for which both strong light-matter interaction and a narrow spectral response are required to achieve high performance.

We propose a photonic-plasmonic cavity with a 1D PhC dielectric cavity vertically coupled to a plasmonic slot. The PhC cavity and the metal slot have been designed in order to maximize the Q/V ratio of the hybrid device. 3D Finite Element Method (FEM) simulations have been carried out to define the cavity performance. We have obtained a Q/V ratio of $7x10^{6}$ $(\lambda/n)^{-3}$ with a high resonance transmission (T = 47 %), that corresponds to an improvement of two orders of magnitude with respect to the state-of-the-art of hybrid cavities. This value of the Q/V ratio is also comparable with the performance obtained by PhC dielectric cavities, but stronger light-matter interactions have been observed in the photonic-plasmonic cavity, due to the ultra-low mode volume $V = 4x10^{-4}$ $(\lambda/n)^{3}$, making the device suitable for biosensing applications, and particularly for optical trapping. In fact, a strong gradient of the optical energy in a very small volume provides high values of optical forces, allowing the trapping of small particles at nanoscale and avoiding direct contact with the trapped object, preserving its disruption or damage. Such performance makes the cavity suitable for several biomedical applications in genetics and proteomics, where trapping, detection and manipulation of proteins, DNA sections and living matter samples smaller than 100 nm is necessary.

2. DEVICE CONFIGURATION

The hybrid device is based on a 1D PhC dielectric cavity in SOI technology vertically coupled to a plasmonic slot in gold (Au) placed above the wire, between the central holes of the PhC, as shown in

Fig. 1. A silica layer is deposited between the PhC cavity and the metal slotted structure to reduce the optical losses, due to the optical absorption in the metal [27].

The silicon nanowire has a width *w* = 490 nm and a thickness *h* = 220 nm. It lays on a silica substrate 1 μm thick. The surrounding medium has been assumed to be water as a fluid carrying a specific particle in biosensing and optical trapping applications [28].

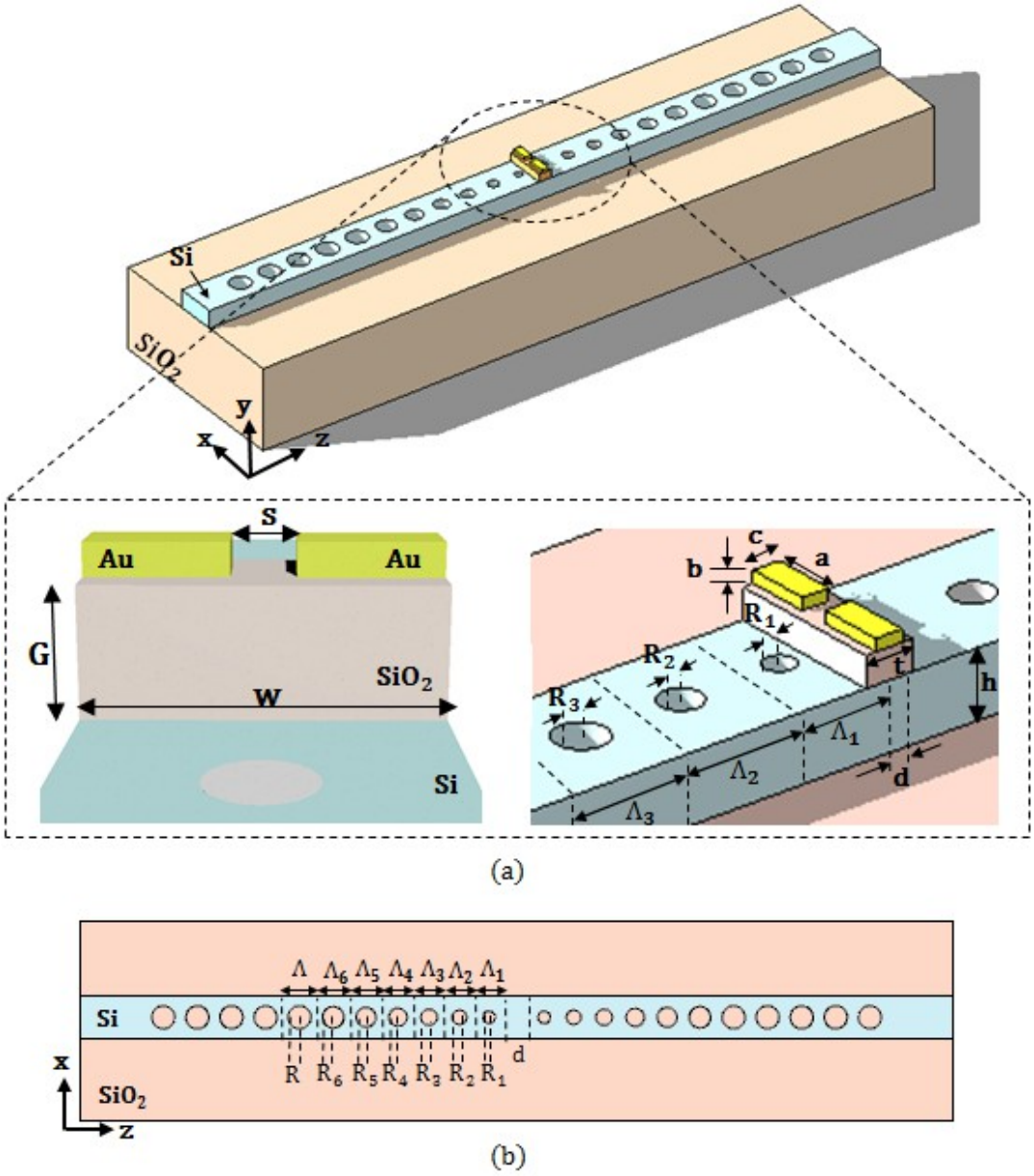

Fig. 1**.** (a)Hybrid device configuration (on the top). The insets highlight the metal slotted structure; (b) Top view of the 1D PhC dielectric cavity of the photonic/plasmonic device configuration.

The cavity consists of two mirror sections, each containing N holes with a fixed radius *R* and a fixed period *Λ*, and a tapering region with N_t holes with different periods $Λ_i$ and radii R_i.

This configuration was designed with the aim of obtaining a resonance condition close to 1550 nm, to minimize the light absorption in the optical fibers and for the availability of source lasers and photodetectors at these wavelengths. The design aims to optimize the energy confinement between the central holes to improve the coupling efficiency between the PhC and the metal slot, and realizing a high resonance transmission in order to avoid the effect of the optical loss contribution due to the metal [29].

Such requirements were met by introducing a tapering section between the cavity and the mirror region, which provides a Gaussian attenuation profile of the optical energy in the PhC cavity, as required by the mode matching condition between the guided mode in the silicon nanowire and the Bloch mode in the PhC. Under this condition, a strong decrease in the optical losses, a higher energy confinement between the central holes, and a higher value of the Q-factor, can be achieved.

A plasmonic nanoantenna was designed above the PhC to funnel the light vertically at resonance. A proper design of the photonic/plasmonic cavity, which provides the overlap between the resonance condition of both cavities, improves the vertical coupling efficiency between the Bloch mode in the PhC cavity to the plasmonic one, enhancing the electromagnetic energy confined in the plasmonic cavity at resonance. In fact, the PhC cavity acts as a mirror at a wavelength inside the photonic bandgap, providing the reflection of light by the mirror holes, except under resonance conditions in which the light propagates along the PhC and is strongly confined in the cavity, between the central holes under the nanoantenna. Therefore, high energy values focused in the cavity interact for a longer time with the plasmonic nanoantennna at resonance due to the several reflections of light in the PhC, so improving the amount of energy that vertically couples to the nanoantenna [27-30].

Moreover, there is a strong refractive index contrast at the interfaces between Au and dielectric materials (SiO_2 and water), so in order to respect the Maxwell equation related to the continuity of the normal component of the electric flux density D ($\hat{n} \cdot (D_{met} - D_{diel}) = 0$), a strong light confinement is typically observed in the material with the lower relative permittivity, which corresponds to water in our

study, with high energy peaks and short penetration depth in metal [31]. The strong subwavelength confinement of the optical energy at the metal edges improves when the gold arms are placed closer to each other, which corresponds to a strong decrease in the mode volume of the hybrid cavity.

The metal slot consists of two rectangular strips in Au separated by a thin region in water. We denote with *a* the length along the x-axis, *b* the thickness, and *c* the side length along the z-axis of each metal layer; *t* is the side length of the silica layer under the plasmonic slot. The width of the metal structure is assumed to be the same as that of the nanowire *w* (see Fig. 1).

The geometrical sizes of the metal layer, the slot width *s* and the distance *G* between the metal and the PhC, i.e. the silica thickness, have been tailored to optimize the coupling efficiency, in order to obtain high values of optical energy at the metal surfaces, by also taking into account the fabrication tolerances.

The presence of the metal slot with a finite length in all directions makes this configuration different from the typical conductor-gap-silicon (CGS) structure [32]. In fact, while in a CGS waveguide a low-loss compact mode propagates in a thin gap of a low-index material sandwiched between a metal layer and a higher-index dielectric layer, our configuration prevents the propagation of the surface plasmon polaritons (SPP) mode and allows strong confinement of the optical energy between the metal strips. The energy is only strongly localized at resonance, because the PhC acts as a mirror at different wavelengths in the photonic bandgap, so that the light is almost totally reflected without any interaction with the slot [27].

The presence of the metal layers causes an increase in optical losses, with a consequent decrease in the Q-factor and the resonance transmission. At the same time, the higher energy confinement results in a decrease of the mode volume, leading to an improvement in the Q/V ratio of about three orders of magnitude with respect to the PhC dielectric cavity without the plasmonic slot because of greater light-matter interaction.

3. DESIGN AND NUMERICAL RESULTS

A high Q/V ratio is requested by several applications, such as biosensing, optical trapping and optical communications [33-36]. The resonance transmission also represents an important figure of merit to define the device performance, because it affects the detection resolution. Therefore, we have designed the proposed photonic/plasmonic cavity in order to maximize the Q/V ratio and the resonance transmission values, as already mentioned.

3.1 *Design of the 1D PhC cavity.*

We designed the PhC dielectric cavity to obtain a very high confinement of the optical energy in the cavity, i.e in the region on which the metal strips are placed, to make the vertical coupling with the plasmonic slot more efficient. The design specifications also include an as high as possible resonance transmission (T ≥ 90%) to overcome the remarkable decrease in T due to the metal absorption which occurs when the PhC cavity constitutes a key element of the photonic/plasmonic device [37].

We considered a period between the mirror holes Λ = 390 nm to obtain a large photonic bandgap that includes the wavelength of 1550 nm. The tapering of the holes and periods allows the distruction of the translational symmetry in the photonic crystal and creates a resonance condition in the photonic bandgap even without the defect *d*, as shown in Fig. 1.

The geometrical and physical parameters of the tapered holes affect the cavity performance, in terms of Q-factor, resonance transmission and resonance wavelength.

We have assumed the filling fraction, $FF_i = \pi \cdot R_i^2 / w \cdot \Lambda_i$, as the parameter for the optimization of the tapered section. Different tapering approaches have been investigated, such as a fixed value, a linear and a quadratic increase in FF from the cavity to the mirror. The best cavity performance was observed with a linear increase in both periods Λ_i and filling fraction FF_i, corresponding to a quadratic increase in the radii of the holes, R_i. In fact, a Gaussian attenuation profile of $|E|^2$ is allowed by this tapering approach, which corresponds to a large decrease in the radiation loss in the cavity, due to better mode matching conditions between the guided mode in the silicon nanowire and the Bloch mode in the PhC.

A parametric analysis was carried out to define the set of values for R_i, Λ_i, N and N_t that optimizes the cavity performance to obtain high values of resonance transmission (T ≥ 90%), energy confinement and Q-factor.

The behavior of the device was simulated using a 3D FEM algorithm, assuming the cavity to be excited by a fundamental TE mode. The wavelength was swept in a wide range from 1500 nm to 1650 nm to evaluate the cavity spectral response. We considered the dispersion of both the Si and SiO_2 refractive index according to the Sellmeier model [38], assuming n_{Si} = 3.478 and n_{SiO2} = 1.444 at 1550 nm. The simulations were carried out by taking into account the presence of water in the surrounding medium (n_{H20} = 1.318 at 1550 nm). The water absorption was also considered, assuming the imaginary part of the refractive index of water to be a function of the operating wavelength (i.e. k = 8.9×10^{-5} at λ = 1550 nm) [39].

The mode volume was evaluated by using the following equation:

$$V = \frac{\iiint_V \varepsilon |E|^2 dV_{cal}}{\max[\varepsilon |E|^2]} \quad (1)$$

where ε is the relative permittivity, $|E|^2$ is the squared module of the electric field and V_{cal} is the whole calculation volume [40].

The influence of R_1 and Λ_1 on the cavity performance is reported in Fig. 2. Different values of the radii R_i and periods Λ_i correspond to any changes in the set of values (R_1, Λ_1), e.g. if (R_1, Λ_1) = (70 nm, 320 nm) then R_2 = 84 nm, R_3 = 96 nm, R_4 = 108 nm, R_5 = 119 nm and Λ_2 = 334 nm, Λ_3 = 348 nm, Λ_4 = 362 nm, Λ_5 = 376 nm, assuming a configuration with N_t = 5 and d = 0 nm, and following a linear increase in both the filling fraction FF and the periods Λ_i.

From Fig. 2, we can observe a significant improvement in Q and the Q/V ratio with increasing R_1 and decreasing Λ_1 (this condition is related to an increase in the radius of all tapered holes that become closer to each other), but also a remarkable decrease in the resonance transmission.

The maximum values of Q and the Q/V ratio obtained with (R_1, Λ_1) = (90 nm, 300 nm) were 5.4×10^4 and 1.4×10^5 $(\lambda/n)^{-3}$, respectively. Unfortunately, they correspond to a very low resonance transmission (T = 3%). This parameter set also provides a resonance wavelength at 1479 nm that is far from the initial requirement chosen for the design (λ_R ~ 1550 nm). A resonance transmission T = 95% was

obtained with (R_1, Λ_1) = (60 nm, 340 nm) (corresponding to smaller tapered holes farther from each other). However, a low Q-factor (= 1.5x10^3), small Q/V ratio (= 1.4x10^3 (λ/n)$^{-3}$), and also a much longer resonance wavelength (λ_R = 1609.9 nm) were achieved by using those geometrical sizes.

A resonance transmission T ≥ 90%, was obtained with R_1 ≤ 70 nm and Λ_1 ≥ 330 nm, and the best compromise in terms of the Q/V ratio and resonance wavelength was observed with R_1 = 70 nm and Λ_1 = 330 nm, providing Q/V = 6.8x10^3 (λ/n)$^{-3}$ and a resonance transmission T = 91% at λ_R = 1589.54 nm, as shown in Fig. 2.

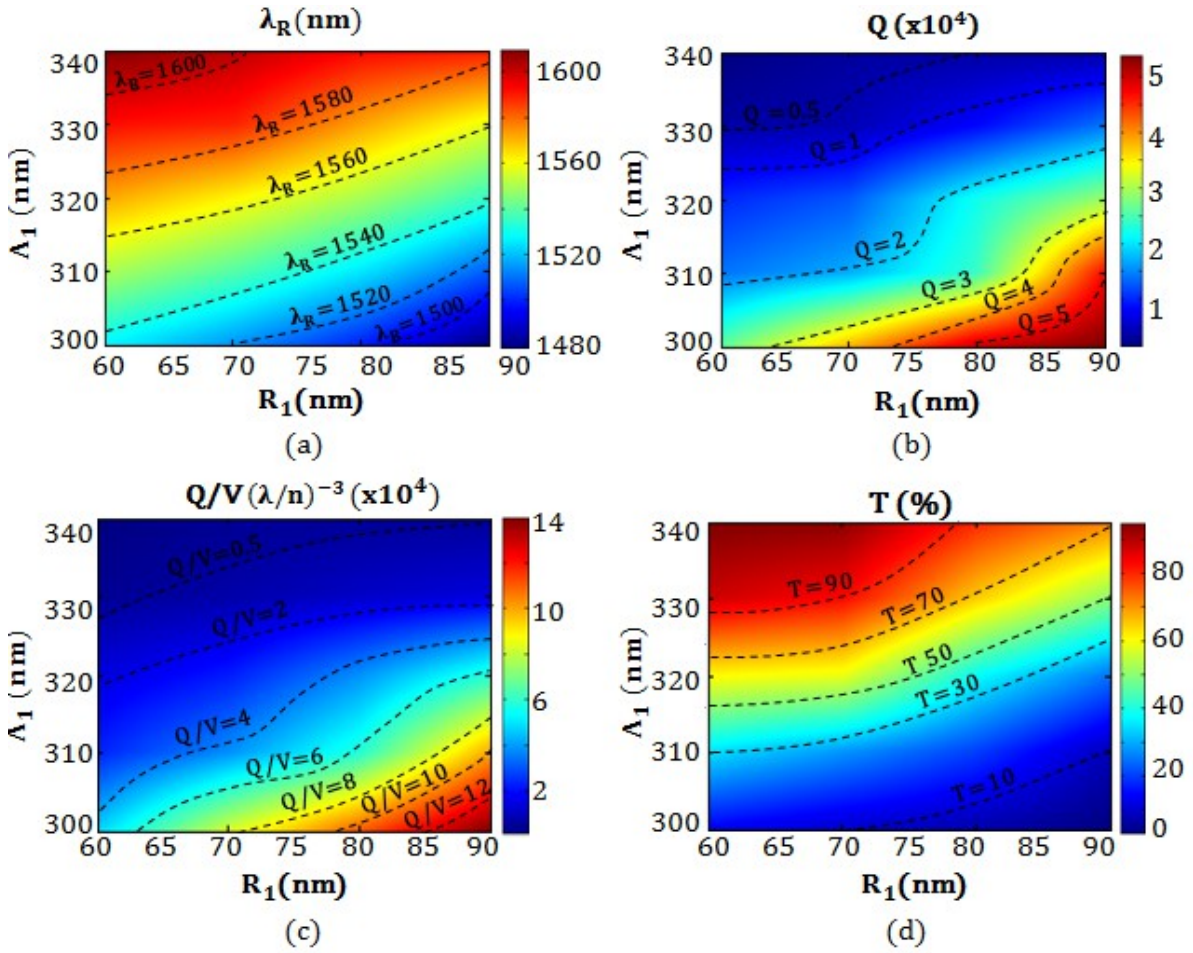

Fig. 2. (a) Resonace wavelength; (b) Q-factor; (c) Q/V ratio; and (d) resonance transmission as a function of the couple (R_1, Λ_1).

The mode distribution in the cavity with these optimized geometrical parameters is reported in Fig. 3. High confinement of the optical energy in the dielectric region between the central holes in resonance condition is clearly shown.

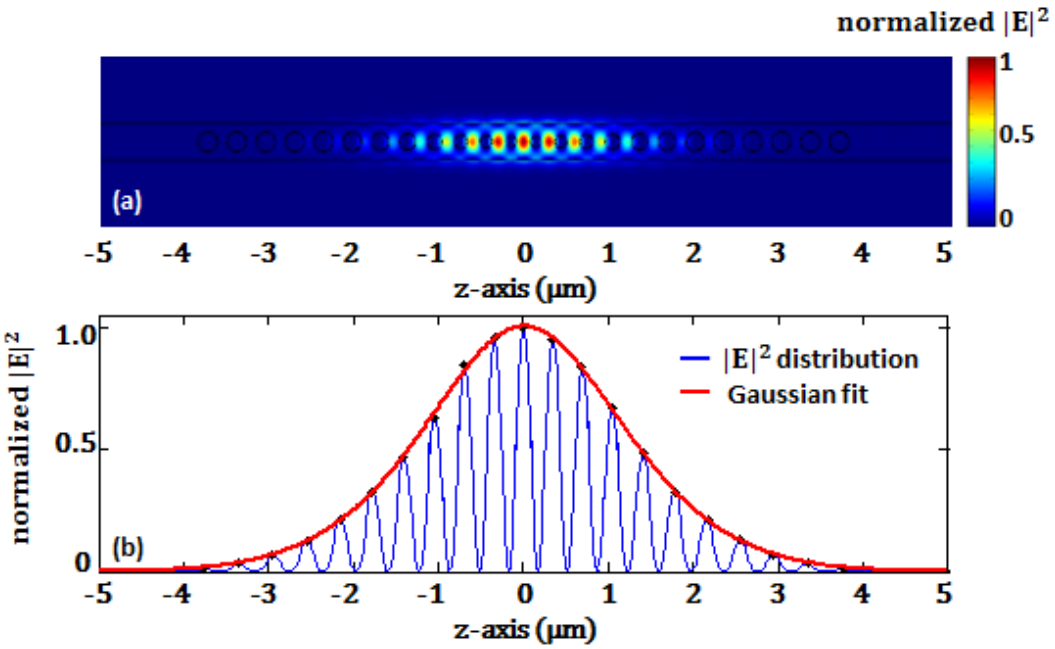

Fig. 3. (a) Distribution of $|E|^2$ in the PhC dielectric cavity with R_1 = 70 nm and Λ_1 = 330 nm, N = 5 and N_t = 6 at resonance λ_R = 1589.54 nm; (b) Comparison between the distribution of $|E|^2$ (blue line) and a Gaussian fit (red line).

A perfect overlap between the $|E|^2$ distribution in the PhC dielectric cavity at resonance (λ_R = 1589.54 nm) and a Gaussian fit was obtained (see Fig. 3.b). A Gaussian attenuation profile corresponds to a minimization of the spatial Fourier harmonics of the cavity mode inside the light cone, which corresponds to a decrease in the radiation loss in free space [9], thus justifying the high value of resonance transmission (T = 91%) obtained with this particular cavity design.

The next step for the optimization of the dielectric cavity was related to the study of the influence on the cavity performance of the defect *d* between the central holes, as shown in Fig. 1.b. This parametric analysis was carried out assuming an initial configuration of the PhC cavity with R_1 = 70 nm and Λ_1 = 320 nm, which provides Q = $1.2\text{x}10^4$, V = 0.58 $(\lambda/n)^3$, corresponding to Q/V = $2.2\text{x}10^4$ $(\lambda/n)^{-3}$, and a resonance transmission T = 59 % at λ_R = 1562.2 nm with *d* = 0 nm.

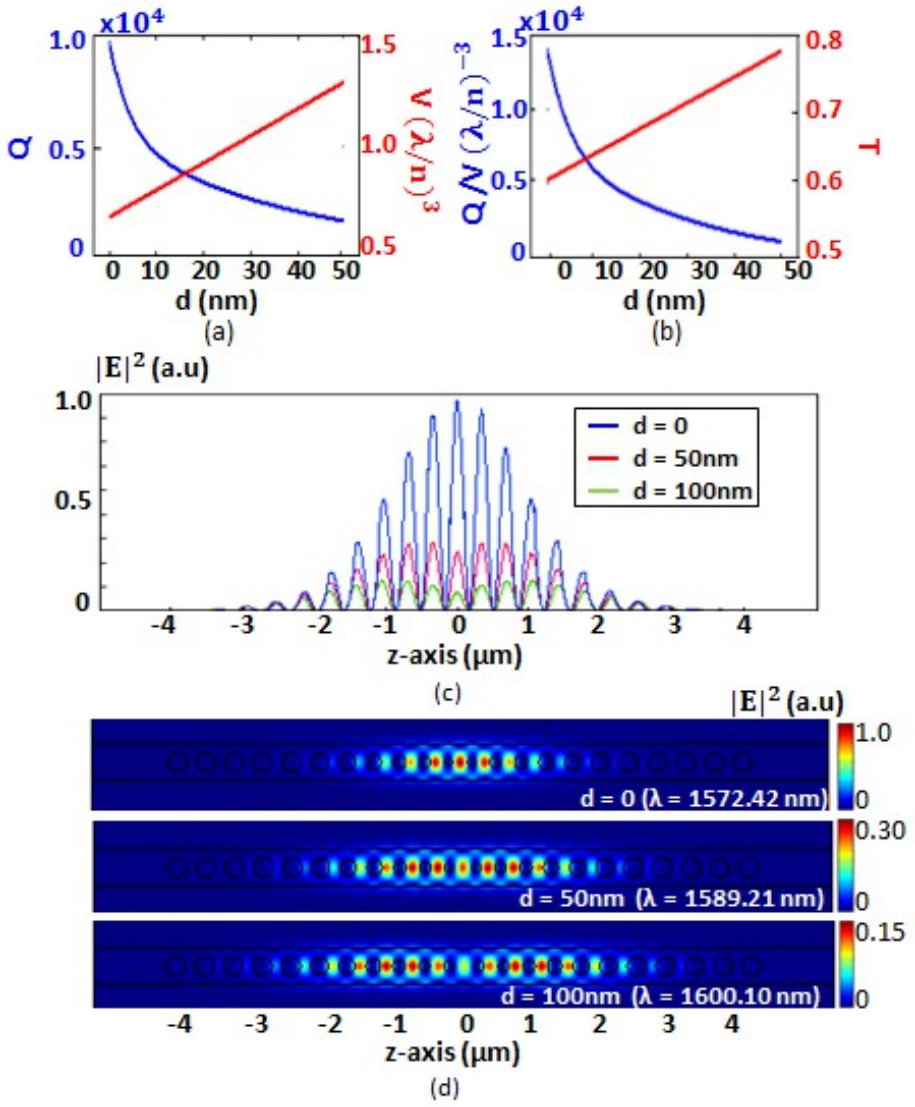

Fig. 4. (a) Quality factor (blue curve) and mode volume (red curve); (b) Q/V ratio (blue curve) and resonance transmission (red curve) as a function of the defect *d;* (c)-(d) $|E|^2$ distribution in the cavity at resonance for d = 0, 50 nm, and 100 nm normalized to the maximum $|E|^2$ peak (*d* = 0 nm).

A significant increase in the resonance transmission was achieved by increasing the defect size, together with a strong decrease in the Q/V ratio, due to the smaller value of Q and, particularly, to an increase in V because of a lower energy confinement in the cavity, as shown in Fig. 4. The best performance was obtained with a null defect (*d* = 0 nm) with a Q-factor of 10^4 and a mode volume V = 0.69 $(\lambda/n)^3$, corresponding to Q/V = 1.4x10^4 $(\lambda/n)^{-3}$ and T = 61 %. A decrease in Q/V of one order of magnitude was measured with *d* = 100 nm with an increase of T up to 76% (see Fig. 4.b).

Such behavior provides lower light-matter interaction and makes the dielectric cavity unsuitable for the hybrid configuration, because the optical energy is more distributed in the photonic crystal when the defect *d* is increased, obtaining the energy peaks between the side holes, as shown in Fig. 4.c and Fig. 4.d. Therefore, we assumed *d* = 0 nm in the device design because of the optimization of the energy confinement in the cavity and the improvement of light-matter interaction.

An important figure of merit in the design of the PhC cavity is the number of the tapered holes N_t. We optimized this parameter to obtain the highest Q-factor which could provide a resonance transmission T ≥ 90%, by using the configuration allowing the best compromise between the resonance transmission and the Q/V ratio (R_1 = 70 nm, R = 130 nm, Λ_1 = 330 nm, Λ = 390 nm and d = 0 nm).

The Q-factor and the resonance transmission T as a function of N_t are reported in Fig. 5.

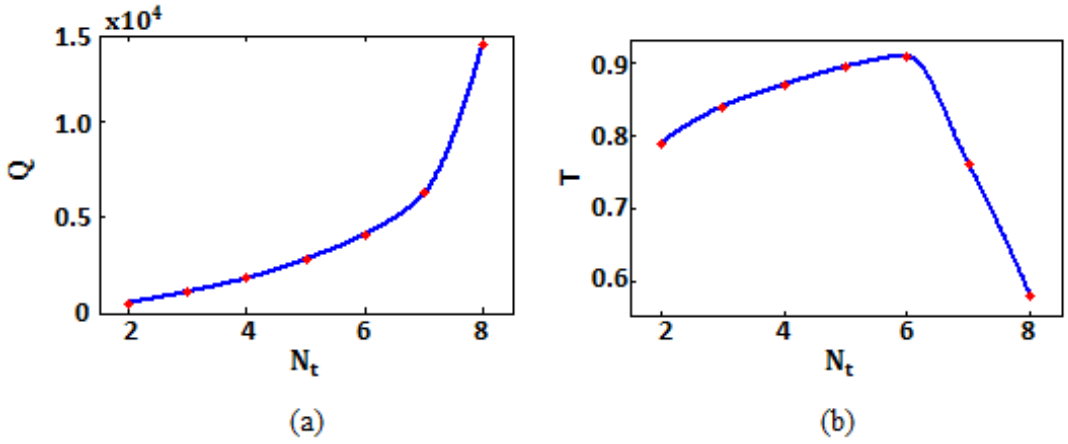

Fig. 5. (a) Q-factor; and (b) resonance transmission behavior as a function of N_t.

A low Q-factor (Q = $5x10^2$) was obtained with N_t = 2, due to a strong mismatch between the guided mode in the nanowire and the Bloch mode. A slight decrease in the radius of the tapered holes and the period from the mirror to the cavity, obtained with a large value of N_t, provides a better mode matching condition, which corresponded to Q ≥ 10^4 with N_t ≥ 8. The resonance transmission increased up to N_t = 6, with a maximum value of T = 91%, while with greater values of N_t a sharp decrease in the resonance transmission was observed (i.e. T = 58% was obtained with N_t = 8). Similar behavior was verified for different values of the radii R_i and the periods Λ_i, demonstrating that the optimized design of the cavity requires N_t = 6. The specification of a resonance condition close to 1550 nm was also

met. In fact, a linear decrease in the resonance wavelength from 1600 nm with N_t = 2 to 1584 nm with N_t = 9 was observed, which corresponds to λ_R = 1589.8 nm with N_t = 6.

The influence of the number of the mirror holes N on the cavity performance in the range from N = 3 to N = 9, was also evaluated, as shown in Fig. 7.

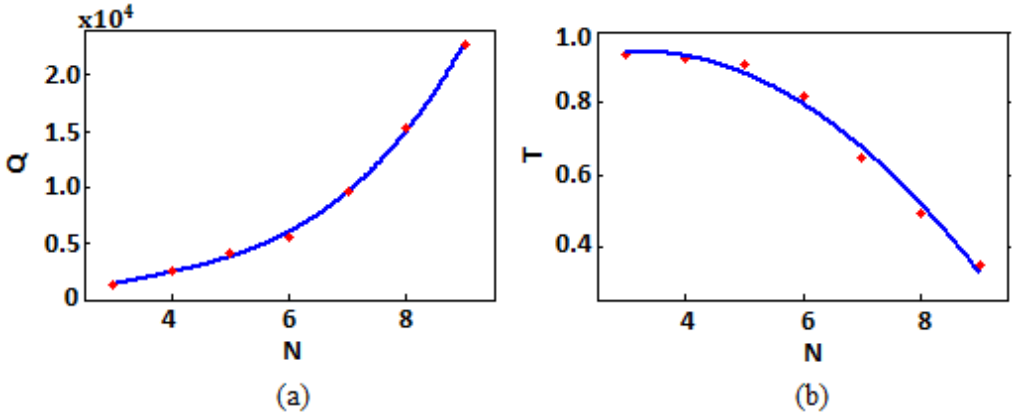

Fig. 6. (a) Q-factor; and (b) resonance transmission behavior as a function of N.

We obtained a quadratic increase in Q, with $Q \geq 10^4$ for $N \geq 7$. In particular, $Q = 2.3 \times 10^4$ with N = 9, which, unfortunately, corresponds to a very low value of T. In fact, the resonance transmission was almost constant ($T \geq 90\%$) up to N = 5 and rapidly decreased up to T = 35% with N = 9. Different values of N did not influence the resonance wavelength.

Assuming N_t = 6, R_1 = 70 nm, R = 130 nm, Λ_1 = 330 nm, Λ = 390 nm and d = 0 nm, we considered N = 5 as the configuration that provides the best compromise between a high Q-factor (= 4.1×10^3) and a low mode volume $V = 0.6\ (\lambda/n)^3$, with $Q/V = 6.8 \times 10^3 (\lambda/n)^{-3}$ and T (= 91%) at λ_R = 1589.8 nm. This configuration of the 1D PhC dielectric cavity was used as the key element of the photonic/plasmonic device.

We also considered the influence of the holes' height on the performance of this particular cavity configuration, which could represent a critical issue in manufacturing the device, due to an incomplete etching process. The depth of all the holes both in the tapering section and in the mirror was denoted as *h'*. We evaluated the cavity performance for several values of *h'* < *h* (= 220 nm). A negligible decrease in T was observed with decreasing *h'*, while Q greatly decreased and a red-shift of the resonance wavelength occurred, i.e. $Q = 3.5 \times 10^3$, and λ_R = 1591.3 nm with *h'* = 210 nm and Q =

$3.1x10^3$, and λ_R = 1593.4 nm with *h'* = 200 nm. Such results confirm the need for a high degree of accuracy in manufacturing the device, particularly during the etching process, to avoid a worsening of the cavity performance.

3.2 *Design of the photonic/plasmonic cavity.*

After the optimization of the 1D PhC dielectric cavity, the metal slot was placed on a silica layer between the central holes of the PhC (see Fig. 1). We took into account the dispersion of Au complex permittivity (ε_{Au}) following the Drude-Lorentz model [41], assuming ε_{Au} = -93.0676+11.1103i at λ = 1550 nm. As for the refractive index of the other materials, we considered the proper value of $\varepsilon_{Au}(\lambda)$.

The design of the metal slot was aimed to optimize the energy confinement between the metal strips in order to maximize the Q/V ratio and the light-matter interaction. The lengths *t* and *c* of the silica and metal layers, respectively, (see Fig. 1) were chosen in relation to the fabrication tolerances. A minimum distance of 30 nm of the edge of the 1st hole from the vertical side of the silica and a minimum metal slot thickness *b* = 20 nm were chosen to meet the manufacturing requirements. Therefore, a fixed value of *t* = 130 nm was assumed in the design, while *c* was determined as the best compromise between the energy confinement and the optical losses in the metal slot. Other geometrical parameters that strongly influence the hybrid cavity performance are the metal thickness *b,* the slot width *s,* and the gap layer *G* (see Fig. 1).

We report in Fig. 7 the influence of the couple of values (*b,c*) on the cavity performance. The parameter *c* was investigated in the range from 50 nm to 80 nm, and *b* from 20 nm to 50 nm. A value of *G* = 100 nm and a slot width *s* = 50nm were assumed, for the optimized configuration of the PhC dielectric cavity with N = 5, N_t = 6, R_1 = 70 nm, *R* = 130 nm, Λ_1 = 330 nm, Λ = 390 nm and *d* = 0 nm.

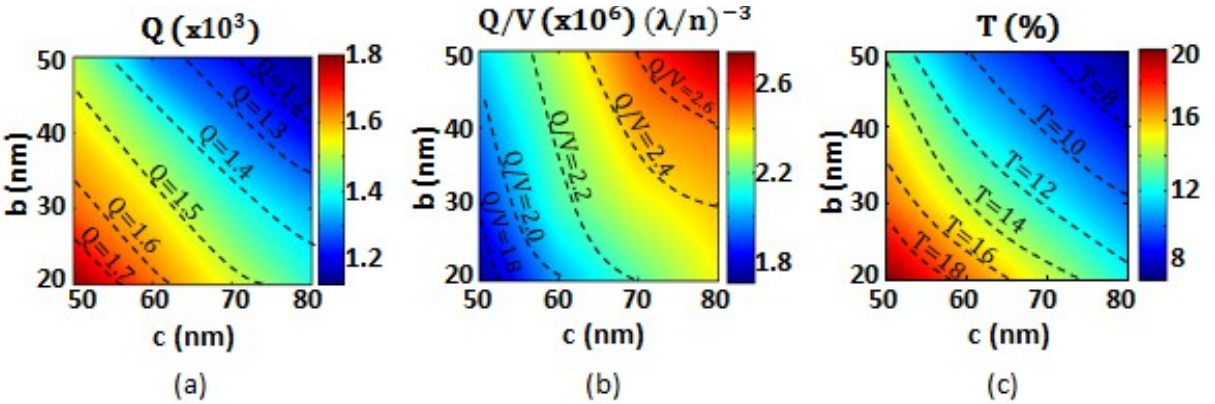

Fig. 7. (a) Q-factor; (b) Q/V ratio ; and (c) resonance transmission as a function of the side length *c* of the silica layer and its thickness b, with *G* = 100 nm and *s* = 50 nm.

We observed a large decrease in T compared to those obtained with the PhC dielectric cavity, at high values of both *b* and c. In fact, a maximum value of T = 20% was achieved by the set (*b,c*) = (20 nm, 50 nm), while T = 7% with (*b,c*) = (50 nm, 80 nm). An increase in the metal sizes also results in a large decrease in the Q-factor from Q = $1.8\text{x}10^3$ with (*b,c*) = (20 nm, 50 nm), up to Q = $1.1\text{x}10^3$ with (*b,c*) = (50 nm, 80 nm), as shown in Fig. 7. The greatest advantage in using the metal slot is related to the large decrease in the mode volume of about three orders of magnitude compared to the values obtained with the PhC dielectric cavity without the metal slotted structure. A maximum value of V = $1\text{x}10^{-3}$ $(\lambda/n)^3$, corresponding to Q/V = $1.7\text{x}10^6$ $(\lambda/n)^{-3}$ with (*b,c*) = (20 nm, 50 nm) was calculated. A decrease in V and a consequent optimization of Q/V was observed on increasing the metal size, up to V = $4\text{x}10^{-4}$ $(\lambda/n)^3$ and Q/V = $2.8\text{x}10^6$ $(\lambda/n)^{-3}$ for (*b,c*) = (50 nm, 80 nm). A slight resonance shift of approximately ten pm was calculated in all cases when varying *b* and *c* in those ranges with respect to the resonance condition obtained with the PhC dielectric configuration (λ_R = 1589.8 nm). Among the sets of values (*b,c*) we investigated, we chose (*b,c*) = (30 nm, 50 nm) as the best compromise, between a higher resonance transmission (= 17%) compared with results in the literature, although with a different pattern of the metal strips, and a mode volume V < $1\text{x}10^{-3}$ $(\lambda/n)^3$ (= $8\text{x}10^{-4}$ $(\lambda/n)^3$), which corresponds to Q/V = $1.9\text{x}10^6$ $(\lambda/n)^{-3}$.

The design of the hybrid configuration was also accomplished with a parametric analysis on the gap *G* and the slot width *s*, as reported in Fig. 8. These parameters were chosen in order to increase the resonance transmission T and thus improve the detection resolution preserving an ultra-high Q/V ratio (> 10^6 $(\lambda/n)^{-3}$).

High optical absorption was observed with small values of *G,* when the metal was close to the PhC cavity, causing a decrease in both the Q-factor and resonance transmission. A reduction in T of 30% between *G* = 200 nm and *G* = 50 nm was observed for each value of the slot width. At the same time, a remarkable improvement in the mode volume of about one order of magnitude was achieved, together with an increase in the Q/V ratio, up to a maximum value of $3.2 \times 10^{6}\ (\lambda/n)^{-3}$ with (*G,s*) = (50 nm, 50 nm). Similar behavior was observed when varying the slot width *s.* In fact, when the metal strips were placed closer to each other, the enhancement of the optical energy in the slot was clear, because the metal assumes a more relevant role. Small values of *s* provide a decrease in the mode volume, a worsening of the Q-factor and higher optical losses. The maximum value of the Q/V ratio (= $3.2 \times 10^{6}\ (\lambda/n)^{-3}$) obtained with (*G,s*) = (50 nm, 50 nm) is one order of magnitude higher than the value obtained with (*G,s*) = (200 nm, 150 nm) that is $Q/V = 3.3 \times 10^{5}\ (\lambda/n)^{-3}$. An increase in the resonance transmission from 8% to 73% was observed, ranging *G* from 50 nm to 200 nm and *s* from 50 nm to 150 nm, as shown in Fig. 8. The resonance wavelength is weakly influenced by the parameters *G* and *s*, and a resonance shift lower than 100 nm was observed for all values in those ranges, with respect to the value obtained with *G* = 100 nm and *s* = 50 nm (λ_R = 1589.8 nm).

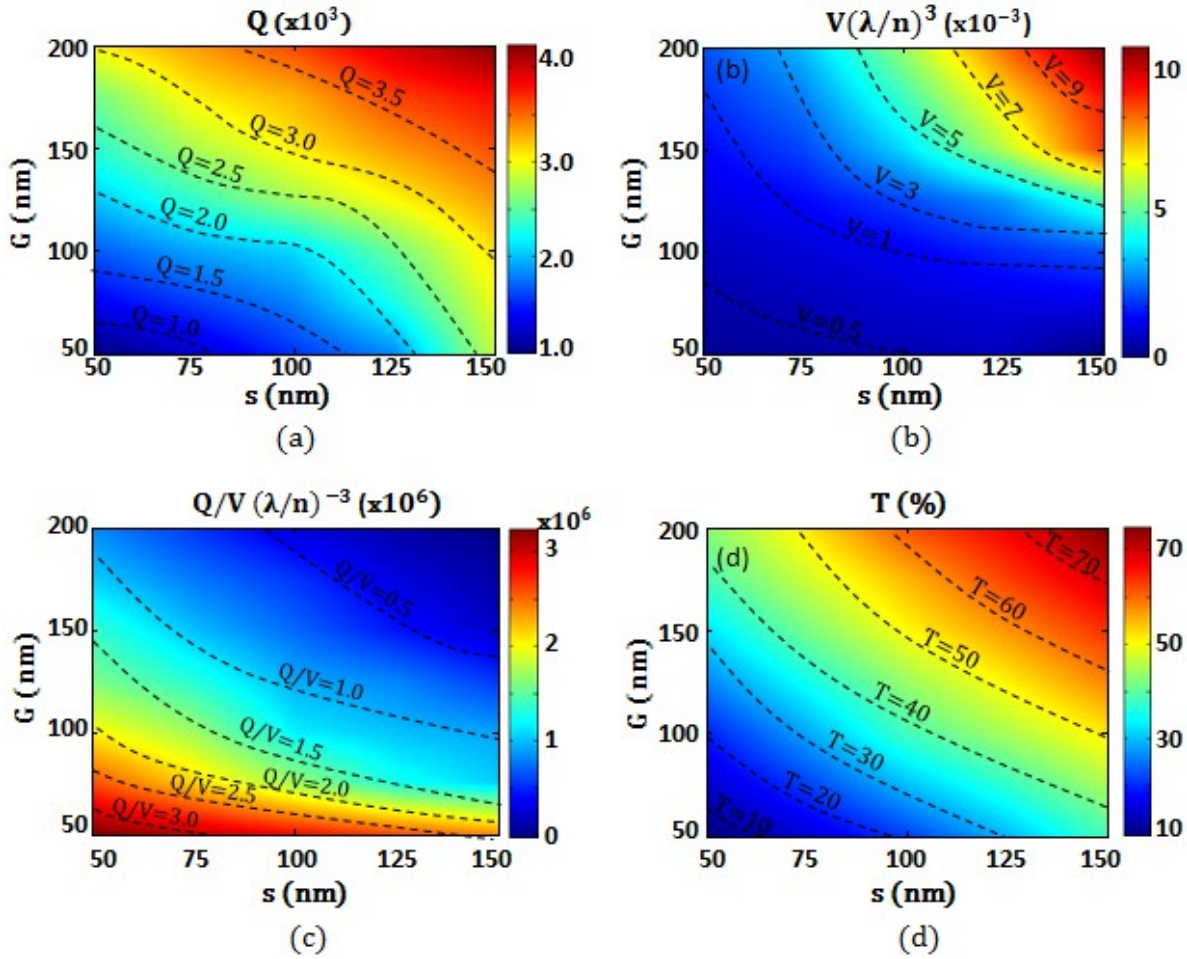

Fig. 8. (a) Q-factor; (b) mode volume; (c) Q/V ratio; and (d) T as a function of the gap *G* and the slot width *s*, with b = 30 nm and c = 50 nm.

We assumed T ≥ 30% as the reference for a good detection resolution and Q/V ≥ 10^6 $(\lambda/n)^{-3}$ to provide strong light-matter interaction. Therefore, *G* = 150 nm, *s* = 50 nm with *b* = 30 nm and *c* = 50 nm represent the best set of parameters to achieve those requirements, obtaining Q = 2.2x10^3, V = 1.5x10^{-3} $(\lambda/n)^3$, which correspond to Q/V = 1.5x10^6 $(\lambda/n)^{-3}$ with T = 30% at λ_R = 1589.8 nm. The spectral response of the hybrid cavity is reported in Fig. 9. The optimized Q/V value of the hybrid cavity is about two orders of magnitude larger than that of the plasmonic nanoantenna without the dielectric cavity. The comparison was carried out using 3D FEM simulations by assuming a dipole Au nanoantenna located directly on a silica substrate and excited by a TE-polarized plane wave from the back-side of the device, under normal incidence conditions.

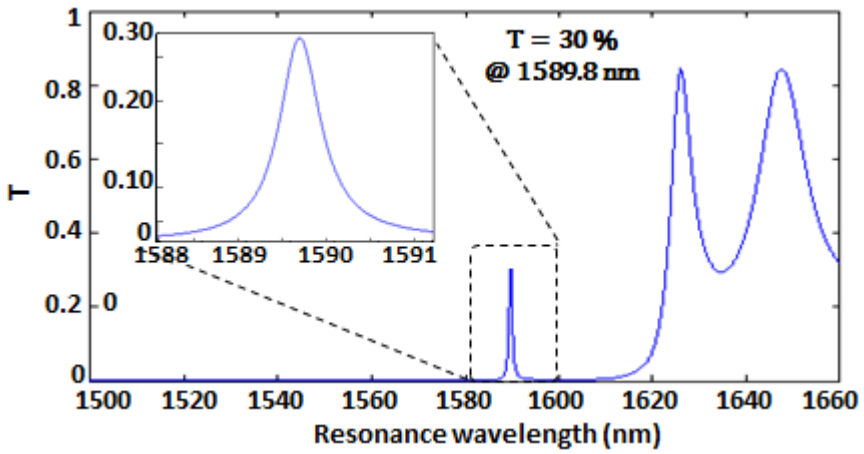

Fig. 9. Transmission spectrum of the hybrid cavity with *s* = 50 nm, *G* = 150 nm and *c* = 50 nm. The inset highlights the spectrum in the wavelength range 1588 nm ÷ 1591 nm with a resonance transmission T = 30 % and Q = 2.2x10^3 at λ = 1589.8 nm.

A decrease of about a factor 2 was obtained with respect to the PhC dielectric cavity from Q = 4.1x10^3 to Q = 2.2x10^3 as well as a good improvement in the mode volume around three orders of magnitude, from V = 0.6 (λ/n)^3 to V = 8x10^{-4} (λ/n)^3.

According to Eq. 1, we calculated ε|E|^2 in the entire domain calculation (3μm x 2μm x 10μm) using 3D FEM simulations with a very fine mesh, obtaining high energy peaks at the corners of the metal structures, which is typical behavior of plasmonic devices. Very dense mesh was used around the whole nanoantenna and also in the silica layer to provide an accurate evaluation of the energy coupled from the PhC cavity.

Therefore, a large decrease in the mode volume was found, in comparison with performance obtained by using dielectric structures, making the enhancement of light-matter interaction in the hybrid cavity remarkable.

These results confirm the increase in the Q/V ratio from Q/V = 6.8 x10^3 (λ/n)$^{-3}$ to Q/V = 1.5x10^6 (λ/n)$^{-3}$, proving the better performance of the photonic/plasmonic cavity, as shown in Tab. 1, and justifying the use of the metal slotted structure to confine higher spatial energy density.

Tab. 1. Comparison of the performance obtained with the PhC dielectric cavity and the photonic/plasmonic one, adding the metal slotted structure.

	Q	V $(\lambda/n)^3$	Q/V $(\lambda/n)^{-3}$	T (%)
Dielectric PhC cavity	$4.1x10^3$	$6x10^{-1}$	$6.8x10^3$	91
Photonic/plasmonic cavity	$2.2x10^3$	$8x10^{-4}$	$1.5x10^6$	30

From the results in Tab.1, an improvement in the Q/V ratio of about two orders of magnitude was obtained, when compared to the performance achieved by other hybrid photonic/plasmonic devices [21]. Moreover, such performance is comparable to the state-of-the-art of PhC dielectric cavities, with the greatest advantage of the higher confinement of the optical energy in the slot filled with water, rather than in silicon as for a typical dielectric configuration, making the device more suitable for sensing and particularly for optical trapping.

The mode distribution in the photonic/plasmonic cavity at resonance is reported in Fig. 10.

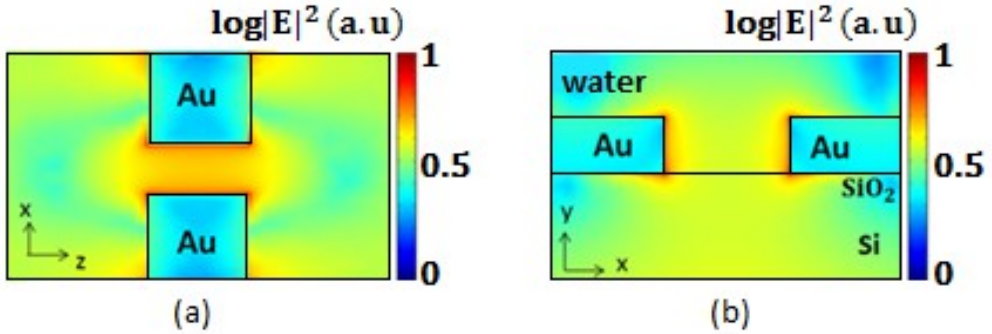

Fig. 10. (a) Top view; and (b) front view of the logarithmic scale of $|E|^2$ around the metal slot in the hybrid device at resonance (λ_R = 1589.8 nm) with *b* = 30 nm, *c* = 50 nm, *s* = 50 nm and *G* = 150 nm.

The metal slot strongly influences the device performance, due to a remarkable energy confinement in the metal slot itself, and particularly at the corners of the gold strips (see Fig. 10). High energy peaks were found in those regions, also reaching values three orders of magnitude higher than the energy values inside the photonic crystal in the hybrid configuration. A decrease of two orders of magnitude in the energy value in the PhC region of the hybrid configuration was observed with respect to the same region without the metal slot. Such behavior corresponds to the high efficiency in the vertical coupling between the dielectric PhC and the metal slot and provides strong light-matter interaction.

Even if the optical energy in the slot represents less than 1% of the total energy distributed in the whole volume, the strong confinement of the optical energy at the metal tips with very high peaks makes the cavity particularly suitable for optical trapping. We expect that a different configuration of the metal slotted structure (i.e. decreasing *G* and *s* to enhance the plasmonic effect) would provide an enhanced energy confinement in the slot, also making the device more suitable for biosensing due to an increase in the sensing region in which the light interacts with the sample.

The results reported in Fig. 7 and Fig. 8 and the energy distribution at resonance in the photonic/plasmonic cavity (see Fig. 10) confirm that the device performance is very sensitive to the pattern of the metal slotted structure. Therefore, we also optimized the shape of the metal structure to increase the energy confinement in the water region between the metal strips and thus improve the efficiency of the hybrid cavity.

We considered a triangular shape for each metal layer, designing a typical configuration of a bowtie shaped nanoantenna [42], as shown in Fig. 11.

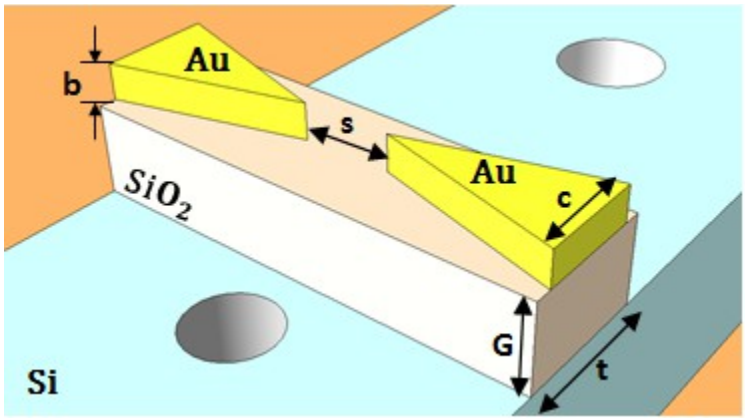

Fig. 11. Bow tie nanoantenna configuration of the metal slot.

Further parametric analysis was carried out to design the configuration of the bow tie, that provides a stronger enhancement of the optical energy in the slot. We kept the side length of the silica layer *t* and the metal thickness *b* constant and equal to 50 nm and 30 nm, respectively, while investigating the influence of the gap layer *G,* the slot width *s,* and the side length of the metal strips *c* on the photonic/plasmonic cavity performance.

We analyzed the influence of *G* in the range from 50 nm to 200 nm, by assuming an initial value of *s* = 50 nm and *c* = 50 nm. The results are shown in Fig. 12.

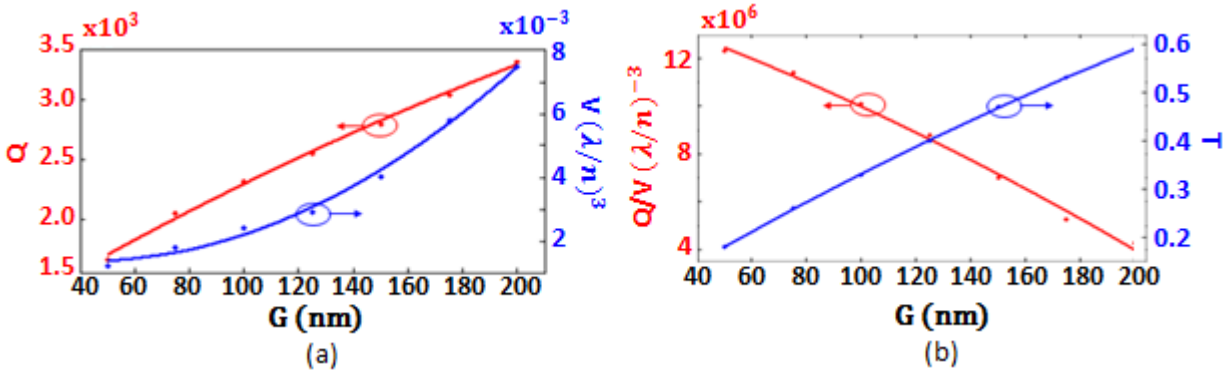

Fig. 12. (a) Quality factor (red curve) and mode volume (blue curve); (b) Q/V ratio (red curve) and resonance transmission (blue curve) of the hybrid device as a function of the gap *G* with a bow tie width *c* = 50 nm and a slot width *s* = 50 nm.

As with the rectangular shape of the metal strips, also in case of a bow tie configuration of the metal slot, an improvement of the Q-factor and of the resonance transmission was achieved with an increase in *G,* due to the lower optical losses caused by the larger distance between the metal and the PhC cavity. A decrease in the energy confinement can be observed, as confirmed by the increase in the mode volume.

Interesting results were obtained by comparing the photonic/plasmonic cavity with a bow tie nanoantenna and a typical dipole configuration with rectangular shapes of the metal layers. An average increase in the Q-factor of around 25% and a decrease in the mode volume, by approximately a factor of 3, were observed with the bow tie structure. Such performance confirms an improvement in the Q/V ratio by a factor 4 for the bow tie configuration, due to stronger light-matter interaction and also to an increase in the resonance transmission of about 15 %.

Similar behavior was observed for Q, Q/V and T as a function of *s,* as shown in Fig. 13. We assumed an initial gap layer *G* = 150 nm and *c* = 50 nm, with *s* ranging from 25 nm to 150 nm.

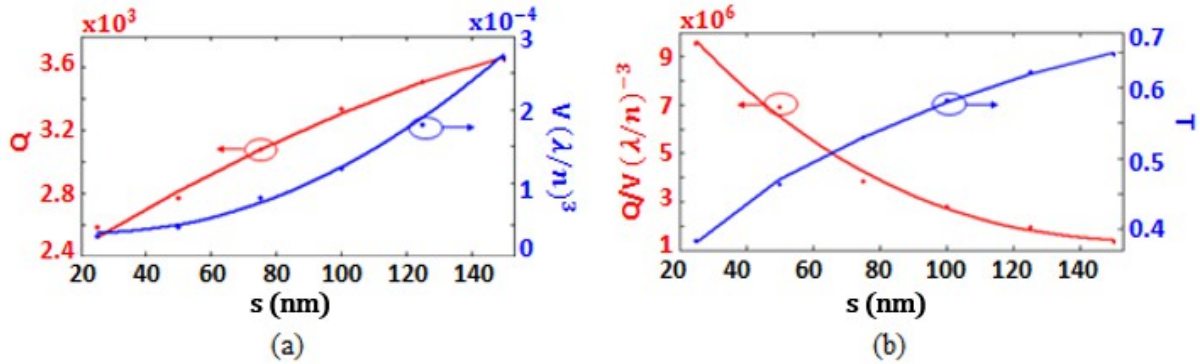

Fig. 13. (a) Quality factor (red curve) and mode volume (blue curve); (b) Q/V ratio (red curve) and resonance transmission (blue curve) of the hybrid device as a function of the bow tie width *s*, assuming *G* = 150 nm and *c* = 50 nm.

A larger bow tie width *s* provides an increase in T, but also a rapid increase in the mode volume, which corresponds to a decrease in Q/V. We assumed *s* = 50 nm as the best compromise between a high detection resolution, strong light-matter interaction and ease of manufacturing. The photonic/plasmonic cavity with *G* = 150 nm, and *s* = 50 nm provides a Q-factor of 2.8×10^3 and a mode volume V = 4×10^4 $(\lambda/n)^3$, corresponding to Q/V = 7×10^6 $(\lambda/n)^{-3}$. The strong improvement in the energy confinement in the bow tie structure provides an increase in the Q/V ratio, allowing the use of a thicker silica layer (*G* = 150 nm) rather than *G* = 100 nm with the dipole configuration, thus reducing the metal absorption and obtaining a higher resonance transmission up to T = 47% at λ_R = 1589.6 nm, still confirming Q/V > 10^6.

An increase in Q/V from Q/V = $1.5 \times 10^6 (\lambda/n)^{-3}$ to Q/V = $7 \times 10^6 (\lambda/n)^{-3}$ as well as an increase in the resonance transmission from T = 30%, with the dipole metal slotted structure, to T = 47% with the bow tie have been measured, demonstrating the higher performance and greater sensitivity of the bow tie, as shown in Fig. 14 and in Tab. 2.

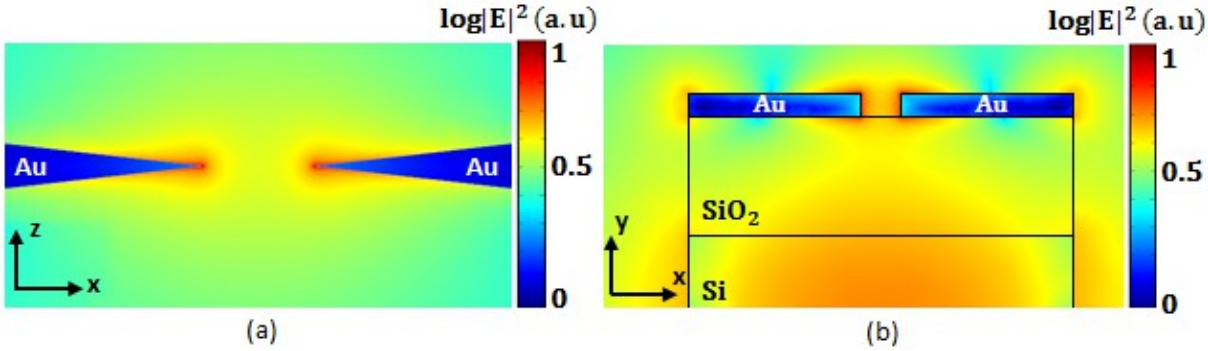

Fig. 14. (a) Top view and (b) front view of the modal distribution in the bow tie at resonance with G = 150 nm, s = 50 nm and c = 50 nm.

The $|E|^2$ distribution shows that the optical energy is more confined in the bow tie, providing greater enhancement of the field by more than one order of magnitude with respect to the dipole configuration.

Tab. 2. Comparison of the performance obtained with the PhC dielectric cavity and photonic/plasmonic configurations 1 and 2.

	Q	V $(\lambda/n)^3$	Q/V $(\lambda/n)^{-3}$	T (%)
Dielectric PhC cavity	$4.1x10^3$	$6x10^{-1}$	$6.8x10^3$	91
Photonic/plasmonic cavity 1 (dipole configuration)	$2.2x10^3$	$8x10^{-4}$	$1.5x10^6$	30
Photonic/plasmonic cavity 2 (*bowtie* configuration)	$2.8x10^3$	$4x10^{-4}$	$7x10^6$	47

Further analysis was carried out to evaluate the influence of the side length of the bow tie on the performance of the photonic/plasmonic cavity (see Fig. 15).

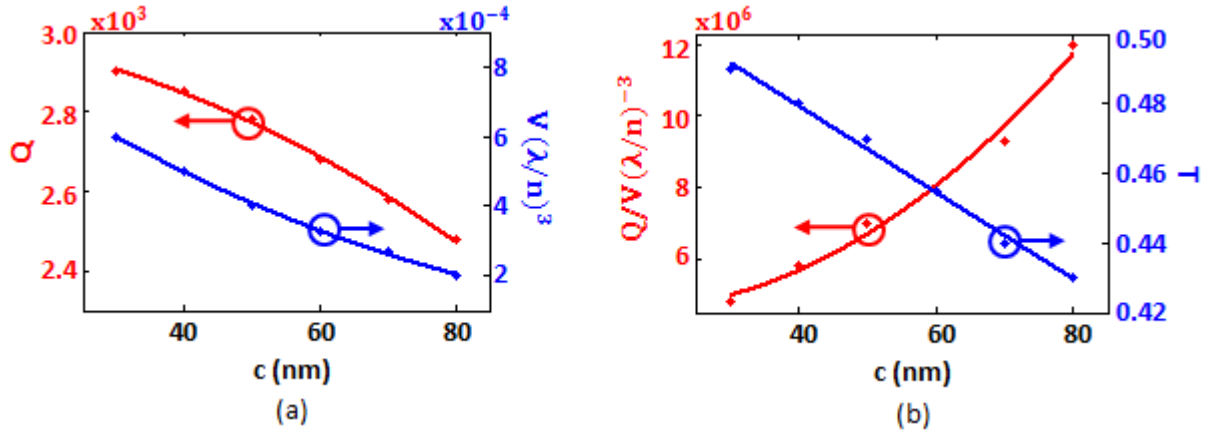

Fig. 15. (a) Quality factor (red curve) and mode volume (blue curve), (b) Q/V ratio (red curve) and resonance transmission (blue curve) of the hybrid device as a function of the side length of the bow tie with s = 50 nm and G = 150 nm.

Greater energy confinement, related to an improvement in the mode volume was observed with an increase in *c*. A mode volume V = $6x10^{-4}$ $(\lambda/n)^3$ was obtained with *c* = 30 nm and V = $2x10^{-4}$ $(\lambda/n)^3$ with *c* = 80 nm. Contrasting behavior of the Q-factor and the resonance transmission were observed, with a slight decrease from Q = $2.9x10^3$ and T = 49% with *c* = 30 nm to Q = $2.5x10^3$ and T = 43% with *c* = 90 nm. Such performance provides a maximum value of the Q/V ratio of $1.2x10^7$ $(\lambda/n)^{-3}$ with a high resonance transmission T = 43% when *c* = 30 nm. We chose a value of *c* = 50 nm as the best compromise between the hybrid cavity performance and fabrication reliability, due to a distance of 40

nm between the bow tie and the vertical edge of the silica layer, thus providing $Q/V > 10^6 (\lambda/n)^{-3}$, and T ~ 50%.

The very high confinement of the optical energy at the metal tips makes the cavity very sensitive to the pattern of the metal structure, and particularly to the sharpness of the tips. We also evaluated the cavity performance with rounded corners of the metal bow tie until *r* = 10 nm, as shown in Fig. 16.

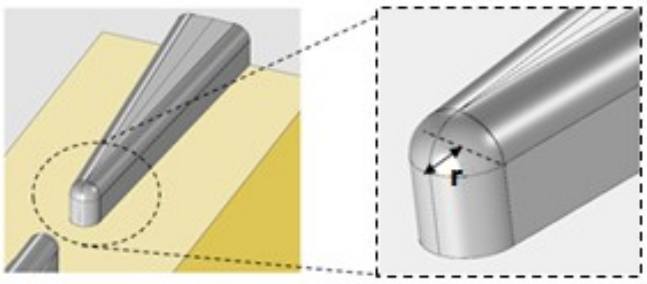

Fig. 16. Configuration of the metal bow tie in the photonic/plasmonic cavity with rounded tips.

A slight decrease in the Q-factor and a particularly relevant increase in the mode volume were achieved by increasing the radius *r*, leading to a decrease in the Q/V ratio. A $Q/V \geq 10^6 (\lambda/n)^{-3}$ was measured with a radius of the rounded tip less than 10 nm. It resulted in $Q/V = 3.3 \times 10^6 (\lambda/n)^{-3}$ and $Q/V = 1.5 \times 10^6 (\lambda/n)^{-3}$ with a radius of 5 nm and 10 nm, respectively.

These results are related to the bow tie configuration, but similar behaviour was also observed using the pattern of a dipole nanoantenna.

This similar behavior confirms the performance to be better than the state-of-the-art hybrid cavities with a more realistic configuration of the bow tie structure.

4. Discussion and conclusions

The rigorous design of a photonic/plasmonic cavity with an ultra-high Q/V ratio to allow strong light-matter interaction has been described in this paper. A 1D PhC dielectric cavity has been optimized with the aim of improving the vertical coupling efficiency with a metal slotted structure. High spectral and spatial density have been achieved, with $Q = 2.2 \times 10^3$, $V = 8 \times 10^{-4} (\lambda/n)^3$, $Q/V = 1.5 \times 10^6 (\lambda/n)^{-3}$, and a resonance transmission T = 30%, with a configuration of the metal slot like a dipole nanoantenna. A further improvement in the hybrid cavity performance has been made by the use of a bow tie structure.

The optimized design of the photonic/plasmonic cavity that provides the best compromise in terms of Q/V ratio, resonance transmission and resonance wavelength was developed with N = 5, N_t = 6, R_1 = 70 nm, R = 130 nm, Λ_1 = 320 nm, Λ = 390 nm, and d = 0 for the design of the PhC dielectric cavity and with a pattern of the metal slotted structure as a typical bow tie nanoantenna with b = 30 nm, c = 50 nm, s = 50 nm and G = 150 nm. This configuration of the hybrid cavity provides a value of Q = 2.8×10^3 and V = 4×10^{-4} $(\lambda/n)^3$, which corresponds to an ultra-high Q/V ratio of 7×10^6 $(\lambda/n)^{-3}$ with a remarkable resonance transmission (= 47%), confirming strong light-matter interaction and a high detection resolution. High values of resonance transmission are especially necessary for biosensing applications and optical trapping, because high signal-to-noise values make it possible to measure smaller changes of resonance transmission in the presence of trapped particles, increasing the device sensitivity while decreasing the minimum detectable size and concentration of living matter.

Such performance also allows high values of energy to be confined in a region at nanoscale with low values of input power. These results confirm an improvement of about two orders of magnitude with respect the state-of-the-art of the hybrid cavities and of about a factor of 6 with respect to dielectric cavities. It corresponds to a higher sensitivity and stronger light-matter interaction with respect to the performance of dielectric and hybrid devices, making the proposed photonic/plasmonic cavity particularly suitable for optical trapping to control and manipulate nanoparticles.

We have shown that the strong gradient of the optical field inside the bow tie provides high optical forces in the pN range, which are required to trap cells of a few microns in size [43] as well as smaller proteins, DNA sections and metal beads (tens of nanometers) [44,45]. Stable optical traps with low input power of a few mW to avoid the thermophoresis effect, can be made. Such performance is not easily attained by other trapping techniques, such as electrophoresis, acoustic and magnetic trapping, thus confirming the suitability of the proposed photonic/plasmonic device for medical applications in proteomics, oncology and genetics, for which stable trapping of small biological nanoparticles, such as proteins, DNA sections and cancer markers, without any disruption or damage is required to allow their analysis and manipulation.

REFERENCES

1) K. J. Vahala, “Optical microcavities”, *Nature*, **424**, 839-846, 2003.
2) C. Ciminelli, F. Dell’Olio, D. Conteduca, C. M. Campanella, and M. N. Armenise, “High performance SOI microring resonator for biochemical sensing”, *Opt. and Las. Tech.,***59**, 60-67, 2014.
3) C. Ciminelli, C. M. Campanella, F. Dell’Olio, C. E. Campanella, and M. N. Armenise, “Label-free optical resonant sensors for biochemical applications”, *Prog. in Quant. Electr.*, **32**(2), 51-107, 2013.
4) Y. Akahane, T. Asano, B.S. Song, and S. Noda, “High-*Q* photonic nanocavity in a two-dimensional photonic crystal”, *Nature*, **425**, 944-947, 2003.
5) R. M. De La Rue, H. Chong, M. Gnan, N. Johnson, I. Ntakis, P. Pottier, M. Sorel, A. M. Zain, H. Zhang, E. Camargo, C. Jin, M. N. Armenise, and C. Ciminelli, “Photonic crystal and photonic wire nano-photonics based on silicon-on-insulator,” *New Jour. of Phys.*, **8**(256), 2006.
6) F. Dell’Olio, C. Ciminelli, D. Conteduca, and M. N. Armenise, “Effect of fabrication tolerances on the performance of two-dimensional polymer photonic crystal channel drop filters: a theoretical investigation based on the finite element method”, *Opt. Eng.,***52**(9), 097104, 2013.
7) H. Sekoguchi, Y. Takahashi, T. Asano, and S. Noda, “Photonic crystal nanocavity with a Q-factor of ~9 million,” *Opt. Exp.*, **22**(1), 916-924, 2014.
8) Y. Taguchi, Y. Takahashi, Y. Sato, T. Asano, and S. Noda, “Statistical studies of photonic heterostructure nanocavities with an average Q factor of three million,” *Opt Exp.,***19**(12), 11916-11921, 2011.
9) Q. Quan, and M. Loncar, “Deterministic design of wavelength scale, ultra-high Q photonic crystal nanobeam cavities,” *Opt. Exp.*, **19**(19), 18529-18542, 2011.
10) H. C. Liu, and A. Yariv, “Designing coupled-resonator optical waveguides based on high-Q tapered grating-defect resonators,” *Opt. Exp.,***20**(8), 9249-9263, 2012.
11) P. Seidler, K. Lister, U. Drechsler, J. Hofrichter, and T. Stöferle, “Slotted photonic crystal nanobeam cavity with an ultrahigh quality factor-to-mode volume ratio”, *Opt. Exp.*, **21**(26), 32468-32483, 2013.

12) Q. Quan, P. B. Deotare, and M. Loncar, “Photonic crystal nanobeam cavity strongly coupled to the feeding waveguide,” *App. Phys. Lett.*, **96**(20), 203102, 2010.

13) K. J. Russel, T. Liu, S. Cui, and E. L. Hu, “Large spontaneous emission enhancement in plasmonic nanocavities,” *Nat.Phot.*, **6**(7), 459–462, 2012.

14) K. J. Russell, and E. L. Hu, “Gap-mode plasmonic nanocavity,” *Appl. Phys. Lett.*, **97**(16), 163115, 2010.

15) Chi-Yu A. Ni, Shu-Wei Chang, S. L. Chuang, and P. J. Schuck, “Quality Factor of a Nanobowtie Antenna”, *J. Ligth. Tech.,* vol. 29, no. 20, pp. 3107-3114, 2011.

16) D. K. Gramotnev, and S. I. Bozhevolnyi, “Plasmonics beyond the diffraction limit”, *Nat. Phot.*, **4**(2), 83-91, 2010.

17) Y. Pang, and R. Gordon, “Optical trapping of a single protein”, Nano Lett. 10(1), pp. 402-406, 2011.

18) D. Punj, M. Mivelle, S. B. Moparthi, T. S. van Zanten, H. Rigneault, N. F. van Hulst, M. F. García-Parajó, and J. Wenger. “A plasmonic ‘antenna-in-box’ platform for enhanced single molecule analysis at micromolar concentrations*”, Nat. Nanotech.,***8**(7), pp. 512-516, 2013.

19) N. Liu, M. L. Tang, M. Hentschel, H. Giessen, and A. Paul Alivisatos, “Nanoantenna-enhanced gas sensing in a single tailored nanofocus”, *Nat. Mater*., **10**(8), pp. 631-636, 2011.

20) E. Eter, T. Grosjean, P. Viktorovitch, X. Letartre, T. Benyattou, and F. I. Baida, “Huge light-enhancement by coupling a bowtie nano-antenna’s plasmonic resonance to a photonic crystal mode”, *Opt. Exp.,* **22**(12), 14464-14472, 2014.

21) X. Yang, A. Ishikawa, X. Yin, and X. Zhang, “Hybrid Photonic-Plasmonic Crystal Nanocavities,” *ACS Nano*, **5**(4), 2831–2838, 2011.

22) M. Barth, S. Schietinger, S. Fischer, J. Becker, N. Nusse, T. Aichele, B. Lochel, C. Sonnichsen, and O. Benson, “Nanoassembled Plasmonic-Photonic Hybrid Cavity for Tailored Light-Matter Coupling”, *Nano Lett.*, vol. **10**(3), pp. 891-895, 2011.

23) A. Di Falco, L. O’Faolain, and T. F. Krauss, “Chemical sensing in slotted photonic crystal heterostructure cavities”, *Appl. Phys. Lett.*, **94**, 063503, 2009.

24) S. Zou and G. C. Schatz, "Combining micron-size glass spheres with silver nanoparticles to produce extraordinary field enhancements for surface-enhanced Raman scattering applications," *Israel J. Chem.,* **46**(3), 293-297, 2006.

25) F. De Angelis, M. Patrini, G. Das, I. Maksymov, M. Galli, L. Businaro, L. Andreani, and E. Di Fabrizio, "A Hybrid plasmonic-photonic nanodevice for label-free detection of a few molecules," *Nano Lett*. **8**(8), 2321-2327, 2008.

26) V. R. Dantham, S. Holler, C. Barbre, D. Keng, V. Kolchenko, and S. Arnold. "Label-free detection of single protein using a nanoplasmonic-photonic hybrid microcavity", *Nano Lett.*, **13**(7), 3347-3351, 2013.

27) C. Ciminelli, D. Conteduca, F. Dell'Olio, and M. N. Armenise, "Design of an optical trapping device based on an ultra-high Q/V resonant structure", *IEEEPhotonics J*., **6**(6), 0600916, 2014.

28) D. Erickson, X. Serey, Y. F. Chen, and S. Mandal, "Nanomanipulation using near field photonics," *Lab on a Chip*, **11**(6), 995-1009, 2011.

29) L. Chen,J. Shakya, and M. Lipson, "Subwavelength confinement in an integratedmetal slotwaveguide on silicon", *Opt. Lett.,* **31**(14), 2133-2135, 2006.

30) C. Ciminelli, F. Dell'Olio, D. Conteduca, T. F. Krauss, and M. N. Armenise, "Hybrid photonic-plasmonic microcavities for Q/V ratio enhancement", 16th International Conference on Transparent Optical networks (ICTON), Graz (Austria), July 6-10, 2014.

31) T. Holmgaard, and S. I. Bozhevolnyi, "Theoretical analysis of dielectric-loaded surface plasmon-polariton waveguides", Phys. Rev. B **75(**245405), 2007.

32) M. Wu, Z. Han, and V. Van, "Conductor-gap-silicon plasmonic waveguides and passive components at subwavelength scale", *Opt. Exp.,* **18**(11), 11728-11736, 2010.

33) J. Joannopoulos, R. Meade, and J. Winn, "Photonic Crystals: Molding the Flow of Light". Princeton, NJ: Princeton Univ. Press, 1995.

34) T. F. Krauss, and R. M. De La Rue, "Photonic crystals in the optical regime - past, present and future," *Prog. in Quant. Electr.*, **23**(2), 51-96, 1999.

35) A. H. J. Yang, S. D. Moore, B. S. Schmidt, M. Klug, M. Lipson, and D. Erickson, "Optical manipulation of nanoparticles and biomolecules in sub-wavelength slot waveguides", *Nature*, **457**, 71-75, 2009.

36) C. Ciminelli, H. M. H. Chong, F. Peluso, R. M. De La Rue, and M. N. Armenise, "High-Q photonic crystal extended microcavity", *European Conference on Optical Communications,* (ECOC2004), Stockholm, Sveden, Sep. 2004.

37) D. Conteduca, F. Dell'Olio, C. Ciminelli, T. F. Krauss, and M. N. Armenise, "Design of a new photonic/plasmonic microcavity allowing a strong light-matter interaction", Third Mediterranean Photonic Conference, Trani (Italy), May 7-9, 2014.

38) I. H. Malitson, "Interspecimen comparison of the refractive index of fused silica," *Jour. of Opt. Soc. Am.*, **55**(10), 1205-1209, 1965.

39) K. F. Palmer, and D. Williams, "Optical properties of water in the near infrared," *Jour. of Opt. Soc. Am.*, **64**(8), 1107-1110, 1974.

40) O. Painter, R. K. Lee, A. Scherer, A. Yariv, J. D. O'Brien, P. D. Dapkus, and I. Kim, "Two-Dimensional Photonic Band-Gap Defect Mode Laser," *Science*, **284**(5421), 1819-1821, 1999.

41) A. D. Rakic, A. B. Djurisic, J. M. Elazar, and M. L. Majewski, "Optical properties of metallic films for vertical-cavity optoelectronic devices," *Appl. Opt.*,**37**(22), 5271-5283, 1998.

42) H. Fisher, and O. J. F. Martin, "Engineering the optical response of plasmonic nanoantennas," *Opt. Exp.*, **16**(12), 9144-9154, 2008.

43) B. S. Ahluwalia, P. McCourt, T. Huser, and O. G. Helleso, "Optical trapping and propulsion of red blood cells on waveguide surfaces", *Opt. Exp.*, **18**(20), 21053-21061, 2010.

44) S. Lin, and K. Crozier, "Trapping-Assisted Sensing of Particles and Proteins Using on Chip Optical Microcavities", *ACS Nano*, **7**(2), 1725-1730, 2013.

45) W. Zhang, L. Huang, C. Santschi, and O. J. F. Martin, "Trapping and Sensing 10 nm Metal Nanoparticles Using Plasmonic Dipole Antennas", *Nano Lett.*, **10**(3), 1006-1011, 2010.

Rigorous design of an ultra-high Q/V photonic/plasmonic cavity to be used in biosensing applications

JOLT_2015_240

Response to reviewers

Reviewer #1

The paper reports theoretical analysis of a hybrid 1D photonic crystal and plasmonic structure that has a high Q/V value and high transmission. The topic is interesting and results are solid and extensive. The paper can be accepted, however, English needs significant imporovement.

We checked the English and modified the manuscript accordingly.